10-1-2003

# Using Optical and Near-Infrared Photometry to Test Macho Lens Candidates

Ted von Hippel
*University of Texas at Austin*, vonhippt@erau.edu

et al.

The Astrophysical Journal, 595:794–802, 2003 October 1


# USING OPTICAL AND NEAR-INFRARED PHOTOMETRY TO TEST MACHO LENS CANDIDATES[1]

Ted von Hippel
Department of Astronomy, 1 University Station C1400, University of Texas, Austin, TX 78712-0259; ted@astro.as.utexas.edu

Ata Sarajedini
Department of Astronomy, 211 Bryant Space Science Center, P.O. Box 112055, University of Florida, Gainesville, FL 32611; ata@astro.ufl.edu

and

Maria Teresa Ruiz
Departamento de Astronomia, Universidad de Chile, Casilla 36-D, Santiago, Chile; mtruiz@das.uchile.cl
*Received 2003 January 27; accepted 2003 June 13*

## ABSTRACT

We obtained new VLT/ISAAC *H*-band observations for five MACHO LMC source stars and adjacent LMC field regions. After combining our near-IR photometry with *Hubble Space Telescope*/PC *BVRI* optical photometry, we compared the MACHO objects to the adjacent field stars in a variety of color-magnitude and color-color diagrams. These diagnostic diagrams were chosen to be sensitive to our hypothesis that at least some of the MACHO lenses were foreground Galactic disk or thick-disk M dwarfs. For the five lensed objects we studied, our hypothesis could be ruled out for main-sequence lens masses $\gtrsim 0.1\ M_{\odot}$ for distances out to 4 kpc. On the other hand, the fact that LMC MACHO 5, an object not in our study, has been recently found to have just such a foreground lens highlights that the remainder of the LMC MACHO objects should be searched for the signature of their lenses using our photometric technique or via near-IR spectroscopy. We also constructed diagnostic color-color diagrams sensitive to determining reddening for the individual MACHO source stars and found that these five objects did not show evidence for significant additional reddening. At least these five MACHO objects are thus also inconsistent with the LMC self-lensing hypothesis.

*Subject heading:* gravitational lensing

## 1. INTRODUCTION

Searches for gravitational microlensing along the line of sight toward the Large Magellanic Cloud (LMC; Paczynski 1986; Udalski, Kubiak, & Szymanski 1997; Alcock et al. 2000a; see also Alfonso et al. 2003) were meant to test for the existence of Galactic dark matter in the form of massive compact halo objects (MACHOs). A handful of gravitational microlensing events toward the LMC with the duration and amplification expected for MACHOs have now been found. Fitting these events into the dark matter picture or into the well-constrained picture of Galactic structure has been problematic, however. For instance, the MACHO collaboration (Alcock et al. 2000a) concluded that they had found 13–17 true microlensing events. After carefully modeling these events and comparing them to known sources of photometric variability that might mimic microlensing as well as known stellar populations along the line of sight to the LMC, Alcock et al. argued that they had detected a previously unknown Galactic halo population of MACHOs with masses between 0.1 and 1 $M_{\odot}$. Assuming the assignment of these objects to the Galactic halo, these MACHOs are abundant enough to account for approximately 20% of the Galactic dark matter implied by dynamical studies. While the implied MACHO mass density is dynamically significant, explaining one-fifth of a problem with no hint regarding the other four-fifths of the problem is deeply unsatisfying. More concretely, a large number of studies have found difficulties with any suggested form of MACHO consistent with the mass range and other properties. For example, the CNO abundance patterns of Galactic stars essentially rule out (Gibson & Mould 1997) the most discussed MACHO candidates, cool white dwarfs. Additionally, a halo of faint M stars is inconsistent with the Hubble Deep Field observations (Gould, Bahcall, & Flynn 1997). If other galaxies contain halo MACHOs in the form of either white dwarfs or M stars, these galaxy halos would be readily observable in the near-IR (Charlot & Silk 1995). Given these difficulties, is there an alternative explanation for the observed microlensing? Some of the events seem to be caused by background supernovae mimicking the expected microlensing light curves (Alcock et al. 2000a), while other events are likely caused by LMC self-lensing. While these photometric variables may account for some of the MACHO sources, we sought to test an additional form of contamination among the MACHO events due to true gravitational microlensing but by a known and possibly underestimated population: M stars from the old disk and thick disk.

The number of Galactic old-disk and thick-disk stars that contribute to the lensing optical depth can be estimated from the local normalizations and scale heights of these populations as well as their mass functions down to approximately 0.1 $M_{\odot}$. Unfortunately, all these parameters except the old-disk normalization and scale height are uncertain. For example, one of the most recent studies to count the faintest, lowest mass Galactic stars (Gould et al. 1997) relied on a color–absolute luminosity relation (Reid 1991) to determine stellar distances and thereby densities. If, however, the stars detected by Gould et al. are subluminous compared to the local sample used by Reid (1991), then the implied density would be much higher. The timescale of

[1] Based on data obtained at ESO (VLT/UT1) under project 66.B-0326.

lensing also is not a meaningful discriminant between lensing by halo and thick-disk objects, as the mean expected values (101 vs. 129 days; Alcock et al. 2000a) differ by too little with the current small samples.

If the MACHO lenses were garden variety old- or thick-disk M stars, there would be clear observable consequences. Such lenses still lie along the line of sight to the LMC sources and would be observable as significant additional near-IR light, measurable as an excess in the near-IR flux of the LMC source. We can check for this near-IR excess by comparing, for example, *H*-band photometry to optical photometry for the MACHO objects. Also, in a matter of time (see below), foreground disk or thick-disk lenses will move through a large enough angle to be detectable as separate objects. Note that our hypothesis is related to but not identical to that of Gates et al. (1998), who argued for the disk as a partial source of dark MACHO lenses.

Assuming our hypothesis is correct, the primary reason we should be able to observe the lens as a near-IR excess is that we expect it to be significantly closer than the LMC, i.e., it should have a distance modulus of ~10–13 versus 18.5 for the LMC. [Disk-star lenses should be distributed according to the combination of population scale height and volume element, which gives a modal distance at 2 times the scale height, i.e., $\sim 2 \times \csc(b) \times 350$ pc and $2 \times \csc(b) \times 1000$ pc for the old and thick disk, respectively. For our viewing angle through the Galactic disk toward the LMC, $\csc(b) = \csc(33^\circ) = 1.8$, so modal disk and thick-disk stars will be found at 1.3 and 3.7 kpc, respectively.] This example also illustrates why we chose to perform this experiment for the LMC sources rather than for the Galactic bulge lensing sources, since the latter have a much smaller distance modulus, approximately 14.5. In addition, the nature of stellar populations along the line of sight to the Galactic bulge is significantly more complex, including the effects of large columns of dust and the Galactic bar.

We decided to search for near-IR excesses only among those lensing sources that are LMC main-sequence stars or slightly evolved subgiants, reasoning that the LMC red giant lensing sources would be too red to notice any near-IR contribution from foreground, line-of-sight Galactic M dwarf lenses. In retrospect, it would have been worthwhile to test our hypothesis against some of the reddest LMC sources as well, and we return to this point later.

## 2. DATA

The MACHO collaboration obtained optical photometry with the Planetary Camera on the *Hubble Space Telescope* (*HST*) to image a number of the LMC lensing sources, in particular, to rule out background supernovae as MACHO mimics. These *HST* data provide the bulk of what we need for our experiment. We selected a sample of six MACHO sources with *HST*/WFPC2 multiband photometry and locations in optical color-magnitude diagrams indicative of being main-sequence or subgiant stars. In addition, all but one of these objects (event 9) pass the stricter lensing candidate selection criteria A of Alcock et al. (2000a), criteria published after we selected our observing sample. Our approach is to supplement the *HST* optical photometry with near-IR photometry. The combination of optical and near-IR photometry allows us to explore M dwarfs as possible lenses with masses as low as 0.1 $M_\odot$ out to 4 kpc or higher mass M dwarfs to greater distances.

### 2.1. *VLT H-Band Data*

We obtained *H*-band queue observations at VLT UT1 using ISAAC (Moorwood 2000) on 2000 November 6–7. The VLT+ISAAC, along with scheduling observations in the queue, allowed us to obtain data that were both photometric and had good image quality—a challenge at the far southern declination (decl. $\approx -70^\circ$) of the LMC but necessary for the relatively crowded LMC fields. We obtained observations for six fields with exposure times ranging from 390 to 780 s and delivered image quality ranging from 2.8 to 4.8 pixels, or 0.″42 to 0.″71 (see Table 1 for details of the observations), along with sky fields taken near the midpoint of the observing sequence. Because of an error (by the PI, not the VLT staff) in the phase II proposal process, one pointing missed the target LMC source, and this field is dropped from further consideration. The *H* band was chosen as the best near-IR compromise between exposure time to a depth of interest and sensitivity to the near-IR excess expected for any line-of-sight M dwarfs.

The ISAAC data were reduced essentially as described in the ISAAC User's Manual.[2] The data were dark subtracted, flat-fielded, sky subtracted, residual bias corrected, bad pixels were found and masked, and then all frames of a given field were registered and averaged. Some image irregularities remained, though these were $\leq 0.5\%$, and at least a fraction of this effect should be additive and thus come out with the sky subtraction during the point-spread function (PSF)-fitting photometry. Given the small range in air-mass values for each field, stacking all images of a given field should not compromise the photometry. For object identification, we used SExtractor (Bertin & Arnouts 1996). Since all five MACHO source objects were at least partially blended with nearby stars, as were the majority of LMC field stars, we employed DAOPHOT II/ALLSTAR (Stetson 1987) to fit empirical PSFs to the reduced and combined *H*-band data. Between 50 and 100 bright uncrowded stars were used to construct the spatially variable PSF on each image. The ALLSTAR routine then iteratively fit the PSF to the central regions of the detected profiles and calculated total magnitudes by integrating the PSFs over their volumes. Using the same 50–100 bright uncrowded stars, we then measured and applied a small, spatially variable aperture correction to the PSF magnitudes to arrive at total aperture magnitudes.

The photometry was calibrated using three standard stars (Persson et al. 1998) observed along with our program, although these standards were observed at lower air-mass values ($X = 1.024$–$1.134$) than our program fields. Since the number of standards observed was too few for a color or

[2] Go to http://www.eso.org/instruments/isaac/.

TABLE 1
LOG OF VLT OBSERVATIONS

| Object | Exposure (s) | DIQ (pixels) | Air Mass |
|---|---|---|---|
| 4..... | 780 | 3.5–4.8 | 1.538–1.560 |
| 6..... | 624 | 2.8–3.4 | 1.511–1.527 |
| 7..... | 780 | 2.8–3.3 | 1.412–1.415 |
| 8..... | 780 | 2.8–3.2 | 1.428–1.436 |
| 9..... | 390 | 3.0 | 1.408–1.411 |
| 14..... | 390 | 3.1–3.7 | 1.600–1.614 |

air-mass term determination, we used the mean *H*-band extinction value for Paranal, 0.06 mag, and assumed a color term of 0.0, as indicated in the ISAAC Data Reduction Guide.[3] Amico et al. expect the *H*-band color term, using *J*–*K* for the color, to be $\leq 0.01$ but have not yet measured its value. We obtained an *H*-band zero point of $24.69 \pm 0.02$. The zero point includes aperture corrections of $-0.015 \pm 0.01$ mag. Uncertainties in the air-mass term of the order of 0.01–0.02 mag per air mass would cause *H*-band offsets of $\sim$0.006–0.012 mag in the extrapolation of the calibration to $X \sim 1.6$ for all stars in the field, whereas a small color term would cause a color-dependent *H*-band offset. While we have no way to estimate the error in the assumed zero-valued color term, if a color term does exist for the *H* band, it would not affect our primary goal of identifying an *H*-band excess for the MACHO sources, since such an excess will be detected relative to the other objects in the field with similar colors.

### 2.2. *HST*/*WFPC2 BVRI Data*

The MACHO team imaged a number of LMC microlensing sources, and these observations are now available in the archive. We used the CADC archive to download the relevant archival images and recalibrate them with the most up-to-date calibration files. Since the *HST* data probed the LMC fields to significantly greater depths than the *H*-band data, we did not always use all of the available *HST* data when a subset in a particular filter had a different roll angle or short exposures. The properties of the data we did use are listed in Table 2. Since the MACHO sources were centered in the PC chip, only the PC data were fully processed. These data were combined and cosmic rays rejected with the IRAF[4] task CRREJ. Sources were found with SExtractor, which also provided morphological classification, allowing us to identify and reject nonstellar objects. The PC images, with a resolution of $\sim$2 pixels or 0.″092 FWHM, were marginally crowded. We were thus able to employ aperture photometry and chose CCDCAP[5] for its subpixel light redistribution and accuracy with small apertures in marginally sampled *HST* data (Mighell 1997). An aperture of 4 pixels was used for all objects in the PC fields, and aperture corrections to 0.″5 (11 pixels = 0.″506) were determined empirically for the brighter objects in each field and filter. As is now well known, the WFPC2 CCDs suffer from a time-dependent charge transfer efficiency (CTE) problem. These exposures were short enough that the background counts on the PC frames ranged from 0 to fewer than 4 counts, and therefore CTE corrections were necessary, especially for the fainter objects and objects at higher *y*-column values. Time-dependent CTE corrections were installed on the basis of the prescription of Dolphin (2000) updated by the data he kindly makes available on his Web site.[6] The CCD dewar window throughput also changes as a function of time and, although such changes are small for these filters (always $<$1.5%), we applied these corrections as well. Finally, we applied the color corrections and zero points to transform the F439W, F555W, F675W, and F814W instrumental magnitudes to standard *B*, *V*, *R*, and *I* magnitudes using the coefficients listed by Dolphin (2000) and updated on his Web page. The photometric transformations of Dolphin are similar to those of Holtzman et al. (1995) but updated for the CTE corrections one first applies and with some additional calibration information. These calibrated *HST* data should be on the *BVRI* system of Landolt (1983, 1992) to within $\pm 0.03$ mag.

The optical PC data were merged with the requirement that an object be detected in at least two filters. The resulting merged photometry lists were then merged with the *H*-band VLT data. Transformations between the PC and VLT reference frames were performed with great care, and typical matches were possible within $\leq$0.3–0.5 ISAAC pixels, depending on the field. In a number of cases, besides the best-matched object on the PC frames, there were one or a few other PC detections within the *H*-band FWHM. During the final merging process, we kept track of all such objects and added their contributed light in each filter if the object would not have been deblended (i.e., if within 3 ISAAC pixels) by the *H*-band PSF-fitting photometry.

Our photometry for the five MACHOs is presented in Table 3. The optical *V* and *I* magnitudes were previously presented by Alcock et al. (2001a). We find a small difference between their and our results of $-0.09 \pm 0.08$ in *V* and $-0.049 \pm 0.02$ in *I*, in the sense of their photometry minus ours. These differences are consistent with our use of updated CTE corrections and photometric transformations.

Since most of the LMC MACHO sources were themselves blended and would not have survived the blending cuts we apply to the remainder of the data (below), we performed a final adjustment to their *H*-band photometry. We carefully examined the location, brightness, and optical colors of objects in the region of each MACHO source on the *HST*/PC and VLT/ISAAC images to determine, as best

[3] The ISAAC Data Reduction Guide v.1.5 by Amico et al. (2002) is available on-line at http://www.eso.org/instruments/isaac/drg/html/drg.html.

[4] IRAF is distributed by the National Optical Astronomy Observatory, which is operated by the Association of Universities for Research in Astronomy, Inc., under cooperative agreement with the National Science Foundation.

TABLE 2
LOG OF *HST* OBSERVATIONS

| Object | Filter | Exposure | Epoch |
|---|---|---|---|
| 4..... | F439W | 1620 | 1999 Aug 19 |
| | F555W | 1590 | 1997 Dec 12 |
| | F675W | 1590 | 1997 Dec 12 |
| | F814W | 16500 | 1997 Nov 12 |
| 6..... | F439W | 1620 | 1999 Aug 26 |
| | F555W | 1620 | 1999 Aug 26 |
| | F675W | 820 | 1999 Aug 26 |
| | F814W | 1040 | 1999 Aug 26 |
| 8..... | F439W | 1600 | 1999 Mar 12 |
| | F555W | 1620 | 1999 Mar 12 |
| | F675W | 820 | 1999 Mar 12 |
| | F814W | 1020 | 1999 Mar 12 |
| 9..... | F439W | 1600 | 1999 Apr 13 |
| | F555W | 1620 | 1999 Apr 13 |
| | F675W | 820 | 1999 Apr 13 |
| | F814W | 1020 | 1999 Apr 13 |
| 14..... | F555W | 2120 | 1997 May 13 |
| | F675W | 2120 | 1997 May 13 |
| | F814W | 2120 | 1997 May 13 |

[5] IRAF implementations of CCDCAP are available via the Web at the following site: http://www.noao.edu/staff/mighell/ccdcap/.

[6] Go to http://www.noao.edu/staff/dolphin/wfpc2_calib/.

TABLE 3
PHOTOMETRY OF MACHO SOURCES

| Object | $B$ | $V$ | $R$ | $I$ | $H$ |
|---|---|---|---|---|---|
| 4..... | $21.73 \pm 0.02$ | $21.41 \pm 0.01$ | $21.17 \pm 0.01$ | $20.90 \pm 0.01$ | $20.28 \pm 0.11$ |
| 6..... | $20.46 \pm 0.01$ | $20.07 \pm 0.01$ | $19.88 \pm 0.01$ | $19.62 \pm 0.01$ | $18.93 \pm 0.03$ |
| 8..... | $20.60 \pm 0.01$ | $20.40 \pm 0.01$ | $20.22 \pm 0.01$ | $20.02 \pm 0.01$ | $19.46 \pm 0.06$ |
| 9..... | $22.28 \pm 0.03$ | $21.39 \pm 0.01$ | $20.79 \pm 0.01$ | $20.38 \pm 0.01$ | $19.16 \pm 0.05$ |
| 14..... | ... | $19.52 \pm 0.01$ | $19.51 \pm 0.01$ | $19.41 \pm 0.01$ | $19.25 \pm 0.06$ |

as possible, the likely contribution of any blended objects that lie within the $H$-band PSFs. We found probable contributions by adjacent objects of $\sim$0.0, 0.2, 0.2, $\leq$ 0.1, and 0.05–0.1 mag in $H$ for LMC MACHO objects 4, 6, 8, 9, and 14, respectively. These expected $H$-band contributions are incorporated into (removed from) the values presented in our figures and discussion, though these corrections are *not* applied to the measured photometry listed in Table 3.

## 3. DISCUSSION

The $VI$ color-magnitude diagram (CMD) for all five LMC fields is presented in Figure 1. The five triangle symbols are the five MACHO microlens source stars. The adjacent field objects are also plotted if their photometric errors were less than 0.1 mag, if any luminosity contributed in the $I$ band from blended objects were $\geq$2.5 mag fainter than the object of interest, and if their morphological classifications from SExtractor were $\geq$0.9. The blending criterion meant that objects which had $\geq$10% luminosity contributions from blended sources in $I$ were excluded. Note that a typically blended object identified as an LMC main-sequence star will have a photometric companion that is also a main-sequence star. The brightest such photometric (line-of-sight) companions will have nearly the same color as the identified object and, thus, will add luminosity more effectively than optical color, much like the observed binary sequences in clusters. The situation is somewhat different for colors composed of optical and $H$-band data, however, since the ground-based $H$-band data had substantially larger PSFs, and thus, objects were generally not blended in the optical PC data but they may be blended in the ISAAC $H$ data. With regard to the morphological classification, although the SExtractor classifier is not strictly Bayesian, the morphology cut removes objects with $\lesssim$90% chance of being point sources. All five fields are overplotted since these LMC fields are only a few degrees apart, and therefore, their distance moduli should be the same within $\leq$0.03 mag (from eq. [13] and the LMC geometry given by van der Marel & Cioni 2001 applied to these field positions). Also plotted are eight model sequences. The left-most isochrone and the isochrone approximately tracing the giant branch are [Fe/H] = $-0.7$ models for log(age) = 8.5 and 9.5 (0.3 and 3.2 Gyr) populations, respectively. We use a 0.3 Gyr model to represent a zero-age main sequence (ZAMS), and the metallicity is chosen to approximate the mean observed value (e.g., see Cole, Smecker-Hane, & Gallagher 2000) for the LMC. The dotted line most visible along the upper main sequence is the expected location of a solar metallicity log(age) = 8.5 (ZAMS) population. The dashed lines from left to right represent the addition to the [Fe/H] = $-0.7$ young isochrone of a 0.1, 0.2, 0.3, 0.4, and 0.5 $M_\odot$ star along the line of sight at a distance of 4 kpc. All models assume a distance modulus to the LMC of 18.5, consistent with Benedict et al. (2002), and $E(B-V) = 0.1$, consistent with Harris, Zaritsky, & Thompson (1997), who found $E(B-V) = 0.13$. We derived the stellar model loci from synthetic photometry of Lejeune, Cuisinier, & Buser (1997) model atmospheres appropriate for each metallicity, effective temperature, and surface gravity for specific Padova (Bertelli et al. 1994) isochrones. The contribution by possible line-of-sight low-mass stars is necessarily approximate, since the mass-luminosity relation for low-mass stars is poorly known. We used the mass-luminosity relation of Henry & McCarthy (1993) supplemented by interpolation of the low-mass main-sequence data presented by Leggett (1992). The line-of-sight stars are assumed to be approximately solar metallicity, as appropriate for Galactic disk stars. Thick-disk or halo stars with lower metallicity would be brighter in both the optical and $H$ bands and so more detectable at any given distance than solar-metallicity stars. Our assumption of solar metallicity for any line-of-sight star is thus conservative in terms of detectability.

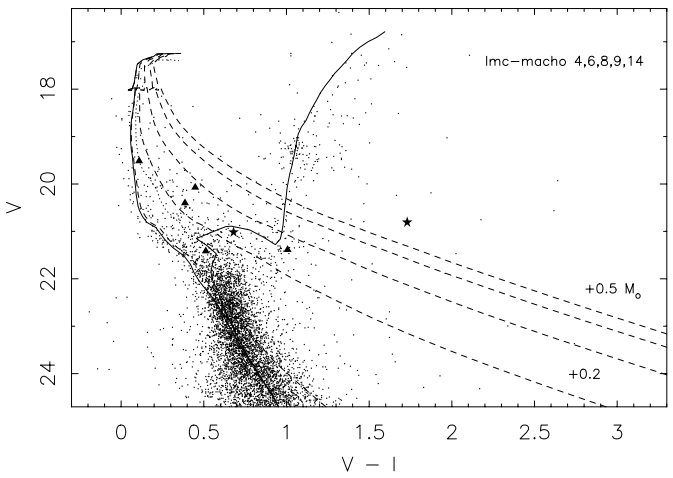


FIG. 1.—LMC MACHO sources (*triangles*) and LMC field stars in the $VI$ CMD. *Far left solid and dotted lines, respectively*: Models based on the Bertelli et al. (1994) isochrones and the Lejeune et al. (1997) model atmospheres for age = 0.3 Gyr with [Fe/H] = $-0.7$ and [Fe/H] = 0.0. A 3.3 Gyr, [Fe/H] = $-0.7$ model is also presented. *Dashed lines*: Models for a combination of the 0.3 Gyr, [Fe/H] = $-0.7$ sequence and 0.1, 0.2, 0.3, 0.4, and 0.5 $M_\odot$ line-of-sight main-sequence disk stars at 4 kpc. *Star symbols*: Expected locations for the source-only and combined photometry for LMC MACHO 5.

Figure 1 reveals LMC field stars with an extended main sequence as well as a subgiant branch, giant branch, and a red clump. The age range of these stars covers at least 0.3–3 Gyr. The location of individual stars is determined by their

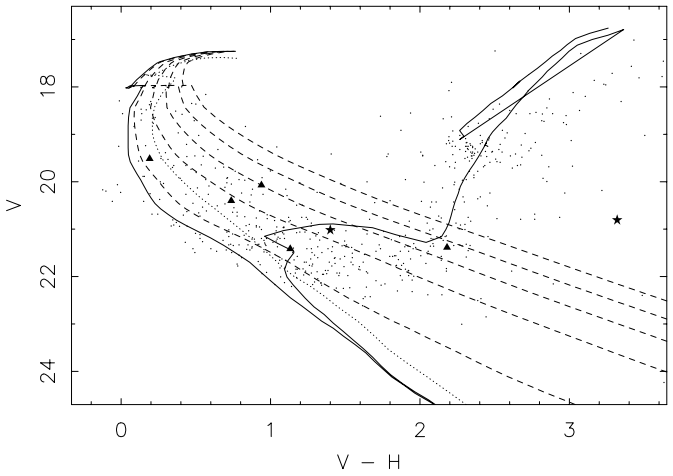


FIG. 2.—LMC MACHO sources and field stars in the *VH* CMD. Symbols have the same meaning as in Fig. 1.

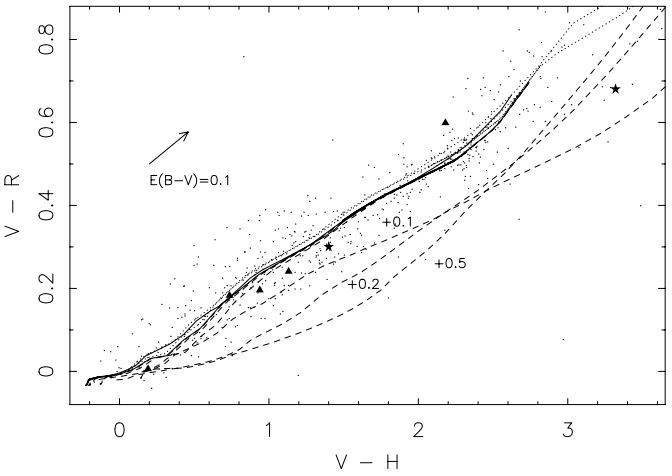


FIG. 4.—*VRH* color-color diagram for the LMC data, ZAMS models, and combination lens+source models. Symbols have the same meaning as in Fig. 3.

abundance and age and possibly also by differential reddening, image blending with other LMC stars, and line-of-sight low-mass star lenses for which we are searching. Two of the MACHO sources appear to be on or near the main sequence, two appear somewhat redder and possibly consistent with a 0.2–0.3 $M_{\odot}$ main-sequence star along the line of sight at 4 kpc, and the remaining object could have a similar explanation or could just be at the base of the giant branch. The *VI* CMD offers too little leverage to test for 0.1 $M_{\odot}$ line-of-sight contributors, as can be seen from the dashed line for the 0.1 $M_{\odot}$ contributor that is minimally offset from the [Fe/H] $= -0.7$ isochrone.

Figure 2 presents the same models and data in the optical+near-IR *VH* CMD with the *H*-band error cut set at less than 0.2 mag rather than at less than 0.1 mag, as is used for the optical bands. Although the models and data now cover a greater color range, this diagram does not break the degeneracy between reddening, evolution away from the main sequence, and a line-of-sight contribution to redness for the MACHO lenses. Figure 3 presents a subset of these data and models in the *VRI* color-color diagram. For clarity, the 0.3 and 0.4 $M_{\odot}$ line-of-sight model sequences have not been plotted and the photometric precision requirements have been tightened to $\leq$0.02 mag in each band. The 1 $\sigma$ photometric errors for the MACHO sources are smaller than the plotting symbols. This color-color diagram is independent of distance and insensitive to reddening, as can be seen by the nearly parallel reddening vector. Likewise unimportant is metallicity: the solar and [Fe/H] $= -0.7$ isochrones are nearly on top of each other. Giants and dwarfs are included in these sequences, and they too lie nearly on top of each other. Except for the bluest object, the MACHO sources all lie among the sequence delineated by the LMC field stars and are consistent with no line-of-sight low-mass star lens, although this color-color diagram is not meaningfully sensitive to lenses with mass as low as 0.1 $M_{\odot}$ at 4 kpc. Figure 4 presents the LMC field stars in the *VRH* color-color diagram, along with the same model stellar sequences. Because of the wide range of the $V-H$ axis and the shallower limits of the *H*-band photometry, the photometry error selection is relaxed to $<$0.2 mag for the *H* band. The 1 $\sigma$ photometric errors for the five MACHO sources range from about half the size to about one and a half times the size of the plotting symbols. The reddening vector is also largely parallel to the stellar sequence in Figure 4, and metallicity has again essentially no effect in this color-color diagram. Now, with greater sensitivity to any low-mass main-sequence lenses, the MACHO source photometry for all but the bluest object is inconsistent with low-mass, lensing main-sequence stars, unless they have masses less than 0.1 $M_{\odot}$ or distances greater than 4 kpc.

With photometry through five filters (*BVRIH*) available to us for four of our five fields and photometry through four filters (*VRIH*) available to us for the remaining (LMC MACHO 14) field, we were able to create a large number of CMDs and color-color diagrams. We do not present these diagrams here as they add little extra insight. The optical CMDs and color-color diagrams all appear to be variations on the themes of Figures 1 and 3, and the *H* band CMDs and color-color diagrams appear to be variations on Figures 2 and 4.

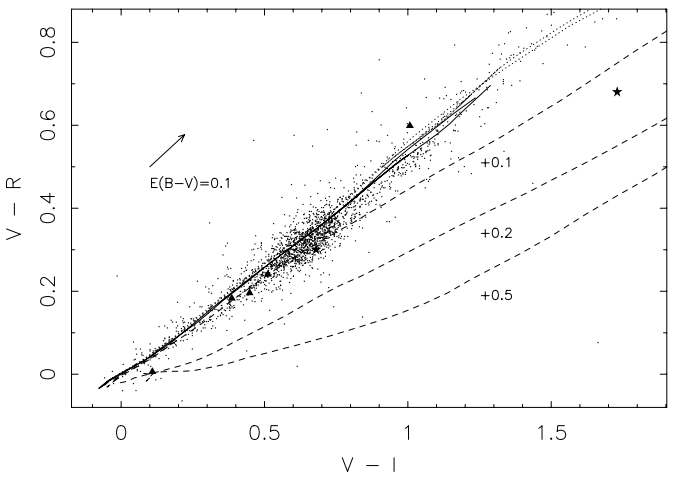


FIG. 3.—*VRI* color-color diagram for the LMC data, ZAMS models, and combination lens+source models. For clarity, the 0.3 and 0.4 $M_{\odot}$ lens models are not presented. The reddening vector for $E(B-V) = 0.1$ is also presented.

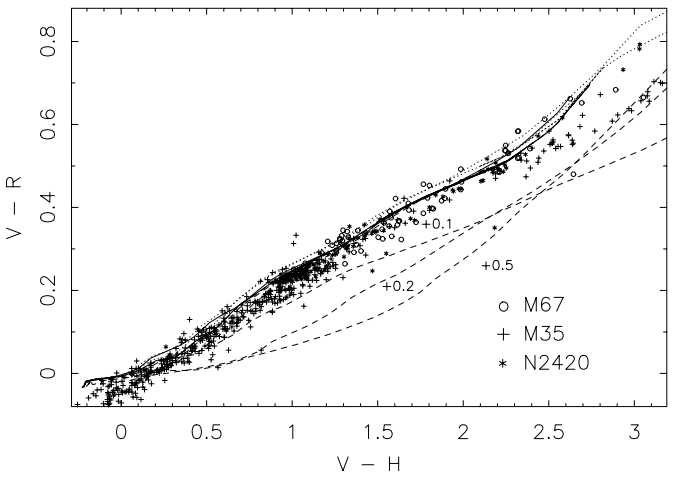


FIG. 5.—*VRH* color-color diagram for the models along with data for the open clusters M35, M67, and NGC 2420.

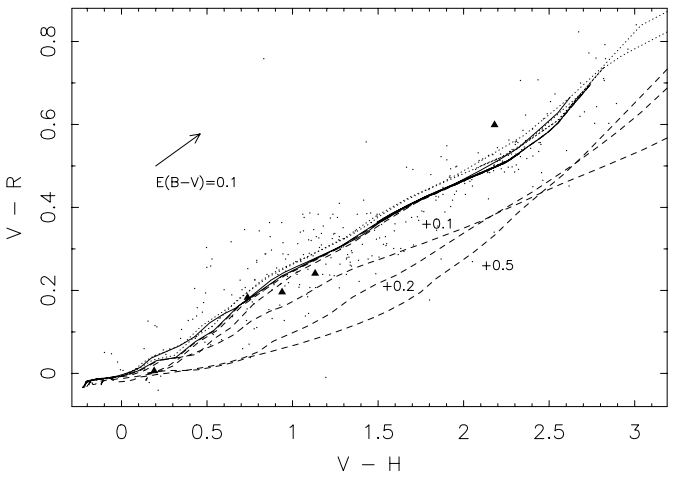


FIG. 6.—*VRH* color-color diagram for the LMC data, ZAMS models, and combination lens+source models, but now the blending threshold has been reduced from 2.5 to 5.0 mag.

Before proceeding on to further interpretation, we verify the location of the model main sequences. In Figure 5, we compare the location of the models to modern photometry for open clusters in the *VRH* color-color diagram. The open cluster data are a combination of optical photometry for M35 (C. P. Deliyannis et al. 2003, in preparation), M67 (Montgomery, Marschall, & Janes 1993), and NGC 2420 (Anthony-Twarog et al. 1990) along with the Two-Micron All-Sky Survey (2MASS) *H*-band photometry merged with the optical data by Grocholski & Sarajedini (2003). The fit is excellent, with only a $\Delta(V-H) \approx 0.1$ mag offset for a given $V-R$ color out to $V-H \approx 2.5$. The CMD fits are also excellent, although there one has the adjustable parameters of distance, metallicity, and reddening.

### 3.1. *Blending*

With 800–2500 stars per LMC *HST*/PC field down to $I \approx 24$, or 0.6–1.8 stars arcsec$^{-2}$, the degree of blending seen in the *H*-band data is expected. For the *HST*/PC with an image quality of $\sim$2 pixels and nearly 500 pixels arcsec$^{-2}$, blending is typically not a problem. The PC data thus provides an excellent indicator for the expected blending in the ISAAC *H*-band data. We used the *I*-band data for the blending measurement since these data are closest in wavelength to the *H*-band data and since the *I* band reaches about 4 mag deeper than the *H*-band data. Thus, for any *H*-band detections more than 1 mag above the *H*-band limit, we are able to determine whether there is any blending contribution to $\leq$1%. In the preceding analysis and plots, we have, however, presented objects with *I*-band blending as large as 10%. Could this $\leq$10% blending, perhaps by intrinsically redder stars that would contribute relatively more in *H* than in *I*, have caused problems in the interpretation? In Figure 6, we present the *VRH* color-color diagram with a blending limit of $\leq$1%. The results are the same, though there are fewer LMC stars to see the general trend. This more stringent blending cut was tested in all CMDs and color-color diagrams, with no net effect on the general location of the LMC field stars.

### 3.2. *LMC Self-Lensing*

The optical depth of LMC self-lensing has been examined in detail by a number of authors (e.g., Sahu 1994; Gyuk, Dalal, & Griest 2000; Zhao 2000). In this section, we examine whether our photometry can constrain the contribution of LMC self-lensing. The addition of the *H* band to the optical data allows us to construct a variety of reddening-free versus reddening-sensitive color-color diagrams. Reddening-free color combinations can be created from any two color combinations linearly differenced in proportion to their reddening ratio. In classic Johnson *UBV* photometry, these reddening-free parameters are abbreviated by *Q* (see Mihalas & Binney 1981). We constructed eight reddening-free indices, which we shall refer to as $Q_1$ through $Q_8$, and plotted those against the $V-H$ color, the longest wavelength baseline color we had for every field. The $V-H$ color is the most sensitive to reddening: $E(V-H) = 2.58\,E(B-V)$. The coefficients in the reddening relations are based on equations (3a) and (3b) of Cardelli, Clayton, & Mathis (1989). The hypothesis we are testing is that many of the lens sources are more distant than the majority of the LMC field stars, which is a prediction of the self-lensing hypothesis, and therefore, on average, they will be more reddened (Zhao 2000). In comparing the lensed stars with objects close to them on the sky in a reddening-sensitive versus reddening-free diagram, the lensing sources should stand out as typically being more reddened. We initially chose as comparison objects all stars within 4″ of the microlens source star but subsequently relaxed the location criterion to the full *HST*/PC field of view since there was no statistical difference in the location of the field stars in this small area versus the entire PC field and since including more objects make it easier to locate the MACHO sources relative to the field LMC stars. Note that reddening due to dust along the line of sight is not the same sort of reddening we were studying above, which would instead be caused by the addition of near-IR light from a much redder object along the line of sight. In various CMDs, either type of reddening might have the same effect, but they can, in principle, be differentiated with the appropriate color-color diagrams.

Of the eight *Q* versus $V-H$ diagrams we constructed, three turned out to have the greatest diagnostic potential

due to the slope of the stellar sequence through the diagram. These three diagrams are presented in Figure 7. The data and model sequences presented in the earlier figures are represented in these reddening-free versus reddening-sensitive color-color diagrams. The MACHO source stars are plotted with their 1 $\sigma$ error bars to distinguish them from the LMC field stars. The three MACHO source stars of intermediate $V-H$ color are consistent in two out of three of these diagrams with the average reddening of the field. In two out of three $Q$ diagrams, the bluest object, near $V-H = 0.2$, is within the envelope of the data but otherwise consistent with a deficit in reddening of $\sim$0.8 in $V-H$ or $\sim$0.3 in $B-V$. Such a deficit in reddening is too large, given the small overall reddening, and is aphysical. All three $Q$ diagrams can be interpreted as implying excess reddening for the reddest MACHO source star, or alternatively, given the shape of the stellar sequences, two out of the three $Q$ diagrams are consistent or marginally consistent with no excess reddening. The large amount of reddening required in the reddening interpretation for this object would equal an additional $E(V-H) \approx 1.5$ or $E(B-V) \approx 0.6$. This is more than necessary to place this object behind the LMC. The most parsimonious explanation for the $Q$ diagrams of the five MACHO source stars is that they have typical reddening for their field and that the color variations seen represent another effect, e.g., photometric blending. We conclude that for these five MACHO sources, there is no significant evidence that they are excessively reddened as one would expect if they had been self-lensed.

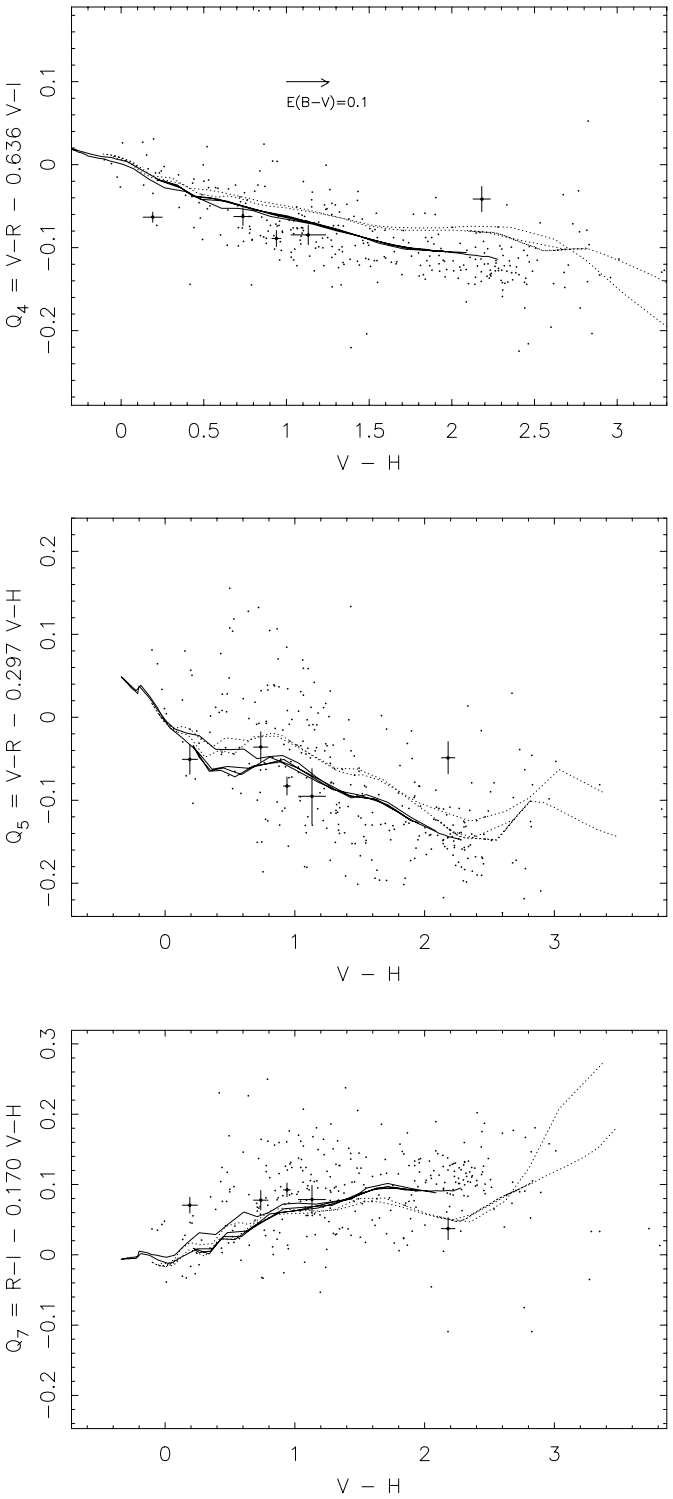


FIG. 7.—$Q$ vs. $V-H$ diagrams for the LMC data and the 0.3 Gyr, [Fe/H] = −0.7 and [Fe/H] = 0.0 models. $Q_4$ (*top*), $Q_5$ (*middle*), and $Q_7$ (*bottom*) are composed of different color-color combinations, as listed on the vertical axes, which are insensitive to reddening. To identify the LMC MACHO source photometry from the field star photometry, the MACHO sources include their 1 $\sigma$ error bars.

### 3.3. *Galactic Main-Sequence Stars as Lenses*

Our experiment was specifically designed to test for the contribution of thin- and thick-disk low-mass dwarfs as MACHO lenses. Our search was sensitive to main-sequence lensing objects with masses $\geq$0.1 $M_\odot$ out to distances of 4 kpc. This statement has been generalized in Figure 8, where we show as a function of LMC source star mass the limiting, or maximum, distance for detecting 0.1, 0.2, 0.3, 0.4, and 0.5 $M_\odot$ main-sequence lenses by our technique. We assume that lensing objects that add $V-H = 0.1$ mag to the color of the source star would be detectable on the basis of the limits found above. We further assume solar-metallicity lenses with the mass-luminosity relation of Henry & McCarthy

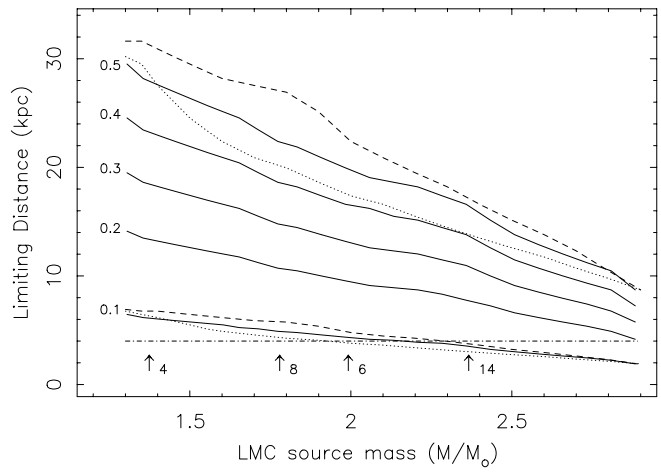


FIG. 8.—Maximum detectable distances for main-sequence lenses of 0.1, 0.2, 0.3, 0.4, and 0.5 $M_\odot$ as a function of the mass of the LMC source star, assumed to have [Fe/H] = −0.7. *Dotted and dashed curves*: For the 0.1 and 0.5 $M_\odot$ case, the same quantities are presented under the assumptions of solar metallicity and [Fe/H] = −1.3 for the LMC source star. *Arrows at bottom*: Expected masses of the listed MACHO source stars. *Dash-dotted line*: Distance equivalent to twice the thick-disk scale height for the Galactic latitude of the LMC.

(1993) and the [Fe/H] = 0.0, −0.7, or −1.3, 0.3 Gyr (Bertelli et al. 1994) isochrones and Lejeune et al. (1997) stellar atmospheres, as used above. These models and assumptions are consistent with the previous analyses. Lower metallicity main-sequence lensing stars would be somewhat brighter for a given mass and therefore easier to detect via our technique. At present, we do not know the metallicities for the LMC MACHO source stars, but it is reasonable to assume that they have approximately the same metallicity as the average star in the LMC. Changes in source star metallicity to solar and [Fe/H] = −1.3 are shown for the 0.5 and 0.1 $M_\odot$ lens cases. The intermediate lens-mass cases look similar and so are not presented to avoid unnecessary crowding in the figure. The region below each line represents the parameter region in which our technique would have detected main-sequence lenses. The horizontal dash-dotted line is placed at 4 kpc, a path length at the Galactic latitude of the LMC of ~2 times the scale height of the thick disk. Four of the five MACHO sources are most likely on the main sequence (see below) or only slightly evolved. Assuming their metallicity to be [Fe/H] = −0.7, their masses are derived by interpolation in our synthetic photometry of the Bertelli et al. (1994) isochrone and Lejeune et al. (1997) atmosphere models. These masses are indicated in Figure 8 by the four arrows. Our technique would have detected the MACHO lenses over a wide range of distance and lens mass, assuming they were main-sequence stars. For three of the MACHOs (4, 8, and 6), such a lens can be ruled out for masses $\geq$0.1 $M_\odot$, and for slightly higher lens masses, even placing the lens in the distant halo would not escape detection. The situation for MACHO 14 is less clear, as indicated in Figures 8 and 4, where this object with a slight $V-H$ excess may match a variety of line-of-sight lens masses. MACHO 9 cannot be so easily compared to an isochrone since one star near the base of the giant branch can match a wide variety of isochrones. On the other hand, in the *VRH* color-color diagram, this object is too blue in $V-H$ for its $V-R$ color. Since this diagram collapses the main sequence, subgiant, and giant stars onto the same color-color sequence, a near-IR excess is still expected for this object if it had a main-sequence lens, though this technique is less sensitive due to the source star's redder color. For the detailed properties of this LMC star, a lensing main-sequence star at 4 kpc with mass = 0.1 or 0.2 $M_\odot$ would produce a $V-H$ excess of 0.06 or 0.19 mag, so the technique remains sensitive down to nearly 0.1 $M_\odot$.

### 3.4. *Details of Individual Lensing Sources*

The above analyses demonstrates that the optical/near-IR colors of the five MACHO source stars studied here are minimally affected or even entirely unaffected by their lenses. The CMD for these stars can then be interpreted in the standard fashion. Object 4 appears to be either a main-sequence star with [Fe/H] > −0.7, or a turnoff star with [Fe/H] ≈ −0.7. Assuming the models we have employed and [Fe/H] = −0.7, its mass is 1.37 $M_\odot$. Object 6 is currently evolving away from the main sequence. For the same model assumptions, its mass is 1.99 $M_\odot$. Object 8 has a mass of 1.78 $M_\odot$ and is also likewise somewhat evolved off the main sequence. Object 9 is the reddest star and is currently at the base of the giant branch. Its main-sequence mass depends on the isochrone fit to this single object, but it is most likely slightly more massive than object 4. The photometry for object 9 is slightly suspect since Alcock et al. (2001a) could not identify which of two adjacent stars had been the lensing source. Both of these objects are fortuitously subgiants, however, so only a small photometric error [$\Delta V = 0.113$, $\Delta(V-I) = 0.011$] would result from assuming the wrong object in the *HST*/PC frames. Object 9 also underwent a binary lensing event (Alcock et al. 2000b). Object 14 appears to be a minimally evolved main-sequence star with a mass of 2.37 $M_\odot$.

Interestingly, we identify faint nebulosity around objects 8 and 14 in the *HST*/PC images. Alcock et al. (2000a) concluded that none of these objects coincided with background galaxies and thus were not supernovae. This assumption should be reexamined for these two objects, though deeper imaging may be required.

### 3.5. *LMC MACHO Candidate 5*

One of the LMC MACHO candidates (5) that is not part of this study was found behind a nearly line-of-sight disk M dwarf star in follow-up *HST*/PC imaging and VLT spectroscopy (Alcock et al. 2001b). This M star was separated from the photometric center of the source star by only 0.″134. Assuming it was the lens gives it a proper motion consistent with the properties of the lens based on the MACHO light-curve analysis. The conclusion of Alcock et al. (2001b) was that finding one such object among the LMC gravitational microlenses was entirely consistent with the expected microlensing optical depth of the Galactic disk population. Here we take a brief detour, using this object as a guide, to ask whether our technique would have discovered this object before it became visually separated on the sky and how long one might have to wait for other such lenses to move far enough away from the line of sight of their source objects to be identified as a separate objects in *HST*/PC photometry.

From the properties listed for this M dwarf star by Alcock et al. (2001b), we can add this object to the *HST* photometry of the LMC MACHO 5 candidate. Unfortunately, different techniques yield different masses for the lensing object. Their constrained lensing fit yields a mass of 0.036 $M_\odot$, and their direct lensing calculation yields a 2 $\sigma$ upper limit mass of 0.069 $M_\odot$. From the lens parameters, they derive a distance of 170–240 pc and $M_V = 15.7$–16.8. On the other hand, the VLT/FORS2 spectrum for the candidate lens indicates that it is a M4–5 dwarf, consistent with the *HST* optical colors. The mass for such an object is significantly higher than their lensing estimates, at 0.095–0.13 $M_\odot$, depending on its metallicity. From the spectrum, they derive $M_V = 13.61 \pm 0.55$ and $d = 650 \pm 190$ pc. We prefer the latter interpretation, under the assumption that the observed object is the lens since the mass and absolute magnitude estimate are based on the observed spectrum and colors. Such an object would be detected by our technique, as is clear from the mass estimate near 0.1 $M_\odot$ and the distance, which is much less than 4 kpc. Under the assumption that the object is an M4 V or M5 V disk star, it would have $V-H = 5.01$–5.84 (Tokunaga 2000), and thus, $M_H = 7.22$–9.15, taking the extremes in the 1 $\sigma$ errors in $M_V$ and the color estimate. Using the observed source and lens optical photometry of Alcock et al. (2001b), a +1 $\sigma$ distance of 840 pc, the lower $H$ flux implied by $V-H = 5.01$, and assuming $V-H$(source) = 1.4, as we see in our LMC field

stars for objects with this source star's $V-I$ color, the expected properties of this object in our CMDs and color-color diagrams are presented in Figures 1–4 with star symbols. In each of these figures, the source star alone is plotted, as well as the photometrically merged object, which is the redder object in all four of these diagrams. If this apparent lensing object were still photometrically merged with this MACHO source, its properties would highlight it as an extremely red object in the CMDs. The *VRI* diagram would be the most indicative of the true properties of this object, although the *VRH* diagram would also indicate a likely foreground low-mass main-sequence star lens. Note that this analysis suggests that the LMC source stars that are apparently redder than any expected stellar sequence (objects 5, 11, 19, 20, and 24 in Alcock et al. 2000a) are prime suspects for lensing by a foreground M dwarf. Secondary suspects are the other red objects (1, 16, 17, 18, and 25).

The Einstein ring radius for an object at 4 kpc is $\sim 5.9 \times (\mathrm{mass})^{1/2}$ mas (see eq. [16] of Paczynski 1986). Assuming this object has a mass of 0.1 $M_{\odot}$, the Einstein ring radius is $\sim$1.9 mas. This is 50 times smaller than the diameter (FWHM) corresponding to the delivered image quality of the *HST*/PC data. A gravitational microlensing event lasting 2 months would correspond to a photometric alignment within the PC image that lasted approximately 8 yr, split evenly between time before and time after the lensing epoch. Typical MACHO lenses should be emerging from photometric alignment with their LMC source stars when viewed at *HST*/PC or *HST*/ACS resolution. The number of photometrically aligned objects that will not become microlenses is even larger, approximately the square of the above radius ratio, or $\sim$625 for the PC image quality. The total MACHO inventory of stars, from among which somewhat more than a dozen lenses were found, contains $\sim 10^7$ stars. Approximately 0.01% of these objects should have photometrically aligned foreground stars at *HST*/PC resolution that will not cause lensing.

## 4. CONCLUSIONS

We obtained new VLT/ISAAC *H*-band observations of a handful of MACHO LMC source stars and adjacent LMC field regions. After combining our new near-IR photometry with *BVRI* optical photometry rederived from *HST*/PC imaging, we compared the MACHO objects to the adjacent field stars in a variety of color-magnitude and color-color diagrams. These diagnostic diagrams were chosen to be sensitive to our hypothesis that at least some of the MACHO lenses were foreground Galactic disk or thick-disk M dwarfs. For the five lensed objects we studied, our hypothesis could be ruled out for main-sequence lens masses $\gtrsim 0.1$ $M_{\odot}$ for distances out to 4 kpc. On the other hand, the fact that LMC MACHO 5, an object not in our study, has been recently found (Alcock et al. 2001b) to have just such a foreground lens highlights that the remainder of the LMC MACHO objects should be searched for the signature of their lenses using our photometric technique or via near-IR spectroscopy. A number of the remaining LMC MACHO objects are excessively red, based on their positions in the MACHO CMD, and these, in particular, should be investigated. We also constructed diagnostic color-color diagrams sensitive to determining reddening for the individual MACHO source stars and found that these five objects did not show evidence for significant additional reddening. At least these five MACHO objects are also inconsistent with the self-lensing hypothesis.

We also recommend an extension of our technique for future MACHO searches: instead of complementing optical photometry with near-IR photometry (or spectroscopy) after the lensing event has passed, these near-IR data could be obtained both during and after the lensing event. Such lensing-event data would break the degeneracy between excess reddening in the source star and the lensing object.

We thank the Canadian Astronomy Data Centre for the archival *HST* data with recalibration and the VLT staff for acquiring the high-quality queue observations. This publication makes use of data products from the Two-Micron All Sky Survey, which is a joint project of the University of Massachusetts and the Infrared Processing and Analysis Center/California Institute of Technology, funded by the National Aeronautics and Space Administration and the National Science Foundation. We also thank Andrew Dolphin for helpful discussions on calibration and Cailen Nelson for MACHO finding charts. A. S. was supported by NSF CAREER grant AST-00 94048. M. T. R. received partial support from FONDAP (15010003), a Guggenheim Fellowship, and Fondecyt (1010404). T. v. H. thanks McDonald Observatory for partial support of this project.

## REFERENCES

Alcock, C. et al. 2000a, ApJ, 541, 270
———. 2000b, ApJ, 542, 281
———. 2001a, ApJ, 552, 582
———. 2001b, Nature, 414, 617
Alfonso, C., et al. 2003, A&A, 400, 951
Anthony-Twarog, B. J., Twarog, B. A., Kaluzny, J., & Shara, M. M. 1990, AJ, 99, 1504
Benedict, G. F., et al. 2002, AJ, 123, 473
Bertelli, G., Bressan, A., Chiosi, C., Fagotto, F., & Nasi, E. 1994, A&AS, 106, 275
Bertin, E., & Arnouts, S. 1996, A&AS, 117, 393
Cardelli, J. A., Clayton, G. C., & Mathis, J. S. 1989, ApJ, 345, 245
Charlot, S., & Silk, J. 1995, ApJ, 445, 124
Cole, A. A., Smecker-Hane, T. A., & Gallagher, J. S. 2000, AJ, 120, 1808
Dolphin, A. E. 2000, PASP, 112, 1397
Gates, E. I., Gyuk, G., Holder, G. P., & Turner, M. S. 1998, ApJ, 500, L145
Gibson, B. K., & Mould, J. R. 1997, ApJ, 482, 98
Gould, A., Bahcall, J. N., & Flynn, C. 1997, ApJ, 482, 913
Grocholski, A., & Sarajedini, A. 2003, MNRAS, in press
Gyuk, G., Dalal, N., & Griest, K. 2000, ApJ, 535, 90
Harris, J., Zaritsky, D., & Thompson, I. 1997, AJ, 114, 1933
Henry, T. J., & McCarthy, D. W. 1993, AJ, 106, 773
Holtzman, J. A., Burrows, C. J., Casertano, S., Hester, J. J., Watson, A. M., & Worthy, G. S. 1995, PASP, 107, 1065
Landolt, A. U. 1983, AJ, 88, 439
———. 1992, AJ, 104, 340
Leggett, S. K. 1992, ApJS, 82, 351
Lejeune, Th., Cuisinier, F., & Buser, R. 1997, A&AS, 125, 229
Mighell, K. J. 1997, AJ, 114, 1458
Mihalas, D., & Binney, J. 1981, Galactic Astronomy: Structure and Kinematics (San Francisco: Freeman), 186
Montgomery, K. A., Marschall, L. A., & Janes, K. A. 1993, AJ, 106, 181
Moorwood, A. T. 2000, From Extrasolar Planets to Cosmology, ed. J. Bergeron & A. Renzini (Berlin: Springer), 12
Paczynski, B. 1986, ApJ, 304, 1
Persson, S. E., Murphy, D. C., Krzeminski, W., Roth, M., & Rieke, M. J. 1998, AJ, 116, 2475
Reid, N. 1991, AJ, 102, 1428
Sahu, K. C. 1994, PASP, 106, 942
Stetson, P. B. 1987, PASP, 99, 191
Tokunaga, A. T. 2000, Allen's Astrophysical Quantities, ed. A. N. Cox (New York: Springer), 151
Udalski, A., Kubiak, M., & Szymanski, M. 1997, Acta Astron., 47, 319
van der Marel, R. P., & Cioni, M.-R. L. 2001, AJ, 122, 1807
Zhao, H. S. 2000, ApJ, 530, 299